

3. The PEP II Storage Rings and Their Impact on the *BABAR* Detector

3.1. PEP-II Storage Rings

PEP-II is an e^+e^- storage ring system designed to operate at a center of mass (c.m.) energy of 10.58 GeV, corresponding to the mass of the $\Upsilon(4S)$ resonance. The parameters of these energy asymmetric storage rings are presented in Table 2. PEP-II has surpassed its design goals, both in terms of the instantaneous and the integrated daily luminosity, with significantly fewer bunches than anticipated. A detailed description of the design and operational experience of PEP-II can be found in references [10] and [11].

Table 2

PEP-II beam parameters. Values are given both for the design and for typical colliding beam operation in the first year. HER and LER refer to the high energy e^- and low energy e^+ ring, respectively. σ_{Lx} , σ_{Ly} , and σ_{Lz} refer to the horizontal, vertical, and longitudinal rms size of the luminous region.

Parameters	Design	Typical
Energy HER/LER (GeV)	9.0/3.1	9.0/3.1
Current HER/LER (A)	0.75/2.15	0.7/1.3
# of bunches	1658	553-829
Bunch spacing (ns)	4.2	6.3-10.5
σ_{Lx} (μm)	110	120
σ_{Ly} (μm)	3.3	5.6
σ_{Lz} (mm)	9	9
Luminosity ($10^{33} \text{ cm}^{-2}\text{s}^{-1}$)	3	2.5
Luminosity (pb^{-1}/d)	135	120

PEP-II typically operates on a 40–50 minute fill cycle. At the end of each fill, it takes about three minutes to replenish the beams. After a loss of the stored beams, the beams are refilled in approximately 10–15 minutes. *BABAR* divides the data into runs, defined as periods of three hour duration or less during which beam and detector conditions are judged to be stable. While most of the data are recorded at the peak of the $\Upsilon(4S)$ resonance, about 12% are taken at a c.m. energy 40 MeV lower to allow for studies of non-resonant

background.

3.2. Impact of PEP-II on *BABAR* Layout

The high beam currents and the large number of closely-spaced bunches required to produce the high luminosity of PEP-II tightly couple the issues of detector design, interaction region layout, and remediation of machine-induced background. The bunches collide head-on and are separated magnetically in the horizontal plane by a pair of dipole magnets (B1), followed by a series of offset quadrupoles. The tapered B1 dipoles, located at ± 21 cm on either side of the IP, and the Q1 quadrupoles are permanent magnets made of samarium-cobalt placed inside the field of the *BABAR* solenoid, while the Q2, Q4, and Q5 quadrupoles, located outside or in the fringe field of the solenoid, are standard iron magnets. The collision axis is off-set from the z -axis of the *BABAR* detector by about 20 mrad in the horizontal plane [12] to minimize the perturbation of the beams by the solenoidal field.

The interaction region is enclosed by a water-cooled beam pipe of 27.9 mm outer radius, composed of two layers of beryllium (0.83 mm and 0.53 mm thick) with a 1.48 mm water channel between them. To attenuate synchrotron radiation, the inner surface of the pipe is coated with a $4 \mu\text{m}$ thin layer of gold. In addition, the beam pipe is wrapped with $150 \mu\text{m}$ of tantalum foil on either side of the IP, beyond $z = +10.1$ cm and $z = -7.9$ cm. The total thickness of the central beam pipe section at normal incidence corresponds to 1.06% of a radiation length.

The beam pipe, the permanent magnets, and the SVT were assembled and aligned, and then enclosed in a 4.5 m-long support tube which spans the IP. The central section of this tube was fabricated from a carbon-fiber epoxy composite with a thickness of 0.79% of a radiation length.

3.3. Monitoring of Beam Parameters

The beam parameters most critical for *BABAR* performance are the luminosity, the energies of the two beams, and the position, angles, and size of the luminous region.

3.3.1. Luminosity

While PEP-II measures radiative Bhabha scattering to provide a fast monitor of the relative luminosity for operations, *BABAR* derives the absolute luminosity offline from other QED processes, primarily e^+e^- , and $\mu^+\mu^-$ pairs. The measured rates are consistent and stable as a function of time. For a data sample of 1 fb^{-1} , the statistical error is less than 1%. The systematic uncertainty on the relative changes of the luminosity is less than 0.5%, while the systematic error on the absolute value of the luminosity is estimated to be about 1.5%. This error is currently dominated by uncertainties in the Monte Carlo generator and the simulation of the detector. It is expected that with a better understanding of the efficiency, the overall systematic error on the absolute value of the luminosity will be significantly reduced.

3.3.2. Beam Energies

During operation, the mean energies of the two beams are calculated from the total magnetic bending strength (including the effects of off-axis quadrupole fields, steering magnets, and wigglers) and the average deviations of the accelerating frequencies from their central values. While the systematic uncertainty in the PEP-II calculation of the absolute beam energies is estimated to be 5–10 MeV, the relative energy setting for each beam is accurate and stable to about 1 MeV. The rms energy spreads of the LER and HER beams are 2.3 MeV and 5.5 MeV, respectively.

To ensure that data are recorded close to the peak of the $\Upsilon(4S)$ resonance, the observed ratio of $B\bar{B}$ enriched hadronic events to lepton pair production is monitored online. Near the peak of the resonance, a 2.5% change in the $B\bar{B}$ production rate corresponds to a 2 MeV change in the c.m. energy, a value that is close to the tolerance to which the energy of PEP-II can be held. However, a drop in the $B\bar{B}$ rate does not distinguish between energy settings below or above the $\Upsilon(4S)$ peak. The sign of the energy change must be determined from other indicators. The best monitor and absolute calibration of the c.m. energy is derived from the measured c.m. momentum of fully reconstructed B mesons combined with

the known B -meson mass. An absolute error of 1.1 MeV is obtained for an integrated luminosity of 1 fb^{-1} . This error is presently limited by the uncertainty in the B -meson mass [13] and by the detector resolution.

The beam energies are necessary input for the calculation of two kinematic variables that are commonly used to separate signal from background in the analysis of exclusive B -meson decays. These variables, which make optimum use of the measured quantities and are largely uncorrelated, are Lorentz-invariants which can be evaluated both in the laboratory and c.m. frames.

The first variable, ΔE , can be expressed in Lorentz invariant form as

$$\Delta E = (2q_B q_0 - s)/2\sqrt{s}, \quad (1)$$

where $\sqrt{s} = 2E_{beam}^*$ is the total energy of the e^+e^- system in the c.m. frame, and q_B and $q_0 = (E_0, \vec{p}_0)$ are the Lorentz vectors representing the momentum of the B candidate and of the e^+e^- system, $q_0 = q_{e^+} + q_{e^-}$. In the c.m. frame, ΔE takes the familiar form

$$\Delta E = E_B^* - E_{beam}^*, \quad (2)$$

here E_B^* is the reconstructed energy of the B meson. The ΔE distribution receives a sizable contribution from the beam energy spread, but is generally dominated by detector resolution.

The second variable is the energy-substituted mass, m_{ES} , defined as $m_{ES}^2 = q_B^2$. In the laboratory frame, m_{ES} can be determined from the measured three-momentum \vec{p}_B of the B candidate without explicit knowledge of the masses of the decay products:

$$m_{ES} = \sqrt{(s/2 + \vec{p}_B \cdot \vec{p}_0)^2 / E_0^2 - p_B^2}. \quad (3)$$

In the c.m. frame ($\vec{p}_0 = 0$), this variable takes the familiar form

$$m_{ES} = \sqrt{E_{beam}^{*2} - p_B^{*2}}, \quad (4)$$

where p_B^* is the c.m. momentum of the B meson, derived from the momenta of its decay products, and the B -meson energy is substituted by E_{beam}^* . Figure 6 shows the m_{ES} distribution for a sample of fully reconstructed B mesons. The resolution in m_{ES} is dominated by the spread in E_{beam}^* , $\sigma_{E_{beam}^*} = 2.6\text{ MeV}$.

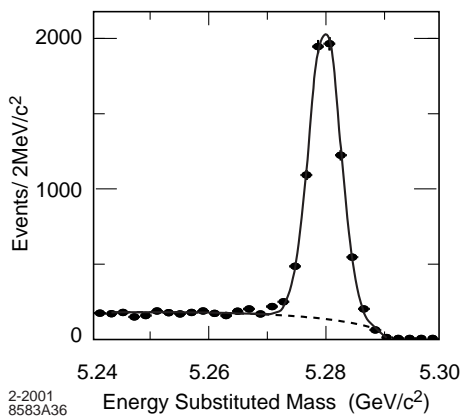


Figure 6. The energy-substituted mass for a sample of 6,700 neutral B mesons reconstructed in the final states $D^{(*)-}\pi^+$, $D^{(*)-}\rho^+$, $D^{(*)-}a_1^+$, and $J/\psi K^{*0}$. The background is extrapolated from events outside the signal region.

3.3.3. Beam Direction

The direction of the beams relative to $BABAR$ is measured iteratively run-by-run using $e^+e^- \rightarrow e^+e^-$ and $e^+e^- \rightarrow \mu^+\mu^-$ events. The resultant uncertainty in the direction of the boost from the laboratory to the c.m. frame, $\vec{\beta}$, is about 1 mrad, dominated by alignment errors. This translates into an uncertainty of about 0.3 MeV in m_{ES} . $\vec{\beta}$ is consistent to within 1 mrad with the orientation of the elongated beam spot (see below). It is stable to better than 1 mrad from one run to the next.

3.3.4. Beam Size and Position

The size and position of the luminous region are critical parameters for the decay-time-dependent analyses and their values are monitored continuously online and offline. The design values for the size of the luminous region are presented in Table 2. The vertical size is too small to be measured directly. It is inferred from the measured luminosity, the horizontal size, and the beam currents; it varies typically by 1–2 μm .

The transverse position, size, and angles of the luminous region relative to the $BABAR$ coordinate system are determined by analyzing the distribution of the distance of closest approach to the z -axis of the tracks in well measured two-track

events as a function of the azimuth ϕ . The longitudinal parameters are derived from the longitudinal vertex distribution of the two tracks. A combined fit to nine parameters (three average coordinates, three widths, and three small angles) converges readily, even after significant changes in the beam position. The uncertainties in the average beam position are of the order of a few μm in the transverse plane and 100 μm along the collision axis. Run-by-run variations in the beam position are comparable to these measurement uncertainties, indicating that the beams are stable over the period of a typical run. The fit parameters are stored run-by-run in the *conditions database*. These measurements are also checked offline by measuring the primary vertices in multi-hadron events. The measured horizontal and longitudinal beam sizes, corrected for tracking resolution, are consistent with those measured by PEP-II.

3.4. Beam Background Sources

The primary sources of steady-state accelerator backgrounds are, in order of increasing importance: synchrotron radiation in the vicinity of the interaction region; interactions between the beam particles and the residual gas in either ring; and electromagnetic showers generated by beam-beam collisions [14–16]. In addition, there are other background sources that fluctuate widely and can lead to very large instantaneous rates, thereby disrupting stable operation.

3.4.1. Synchrotron Radiation

Synchrotron radiation in nearby dipoles, the interaction-region quadrupole doublets and the B1 separation dipoles generates many kW of power and is potentially a severe background. The beam orbits, vacuum-pipe apertures and synchrotron-radiation masks have been designed such that most of these photons are channeled to a distant dump; the remainder are forced to undergo multiple scatters before they can enter the $BABAR$ acceptance. The remaining synchrotron radiation background is dominated by x-rays (scattered from tungsten tips of a mask) generated by beam tails in the high-field region of the HER low- β quadrupoles. This residual back-

ground is relatively low and has not presented significant problems.

3.4.2. Beam-Gas Scattering

Beam-gas bremsstrahlung and Coulomb scattering off residual gas molecules cause beam particles to escape the acceptance of the ring if their energy loss or scattering angle are sufficiently large. The intrinsic rate of these processes is proportional to the product of the beam current and the residual pressure (which itself increases with current). Their relative importance, as well as the resulting spatial distribution and absolute rate of lost particles impinging the vacuum pipe in the vicinity of the detector, depend on the beam optical functions, the limiting apertures, and the entire residual-pressure profile around the rings. The separation dipoles bend the energy-degraded particles from the two beams in opposite directions and consequently most *BABAR* detector systems exhibit occupancy peaks in the horizontal plane, *i.e.*, the LER background near $\phi = 0^\circ$ and HER background near $\phi = 180^\circ$.

During the first few months of operation and during the first month after a local venting of the machine, the higher pressures lead to significantly enhanced background from beam-gas scattering. The situation has improved significantly with time due to *scrubbing* of the vacuum pipe by synchrotron radiation. Towards the end of the first year of data-taking, the dynamic pressure in both rings had dropped below the design goal, and the corresponding background contributions were much reduced. Nevertheless, beam-gas scattering remains the primary source of radiation damage in the SVT and the dominant source of background in all detectors systems, except for the DIRC.

3.4.3. Luminosity Background

Radiative Bhabha scattering results in energy-degraded electrons or positrons hitting aperture limitations within a few meters of the IP and spraying *BABAR* with electromagnetic shower debris. This background is directly proportional to the instantaneous luminosity and thus is expected to contribute an increasing fraction of the total background in the future. Already this is

the dominant background in the DIRC.

3.4.4. Background Fluctuations

In addition to these steady-state background sources, there are instantaneous sources of radiation that fluctuate on diverse time scales:

- beam losses during injection,
- intense bursts of radiation, varying in duration from a few ms to several minutes, currently attributed to very small dust particles, which become trapped in the beam, and
- non-Gaussian tails from beam-beam interactions (especially of the e^+ beam) that are highly sensitive to adjustments in collimator settings and ring tunes.

These effects typically lead to short periods of high background and have resulted in a large number of *BABAR*-initiated beam aborts (see below).

3.5. Radiation Protection and Monitoring

A system has been developed to monitor the instantaneous and integrated radiation doses, and to either abort the beams or to halt or limit the rate of injection, if conditions become critical. In addition, DCH and IFR currents, as well as DIRC and IFR counting rates, are monitored; abnormally high rates signal critical conditions.

Radiation monitoring and protection systems are installed for the SVT, the DCH electronics, and the EMC. The radiation doses are measured with silicon photodiodes. For the SVT, 12 diodes are arranged in three horizontal planes, at, above, and below the beam level, with four diodes in each plane, placed at $z = +12.1$ cm and $z = -8.5$ cm and at a radial distance of 3 cm from the beam line [17]. The diode leakage current, after correction for temperature and radiation damage effects, is proportional to the dose rate. The four diodes in the middle are exposed to about ten times more radiation than the others. These mid-plane diodes are connected to the beam abort system, while the remaining eight diodes at the

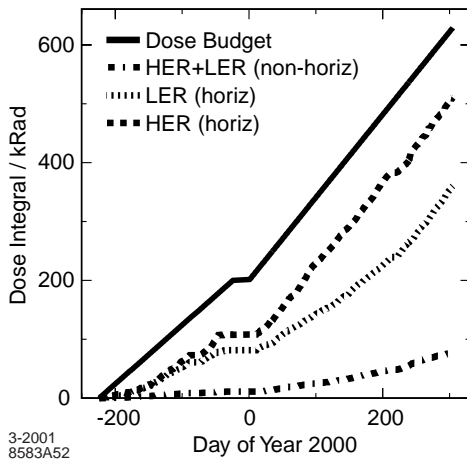


Figure 7. The integrated radiation dose as measured by PIN diodes located at three different positions, showing contributions from the HER ($\phi = 180^\circ$), and the LER ($\phi = 0^\circ$) in the horizontal plane, and from both beams combined elsewhere. Also shown is the SVT radiation budget for the first 500 days of operation.

top and bottom are used to monitor the radiation dose delivered to the SVT. The accuracy of the measured average dose rate is better than 0.5 mRad/s. The integrated dose, as measured by the SVT diodes, is presented in Figure 7.

The radiation level at the DCH and the EMC is more than two orders of magnitude lower than at the SVT. To amplify the signal, the PIN diodes for the DCH and EMC are mounted on small CsI(Tl) crystals (with a volume of about 10 cm^3). These silicon diodes are installed in sets of four. Three sets are mounted on the front face of the endcap calorimeter and one set on the backward endplate of the DCH, close to the readout electronics. The signals of the four diodes in each set are summed, amplified, and fed into the radiation protection electronics. Only one of the three diode sets of the EMC is used at any given time. The DCH and the EMC use identical hardware and decision algorithms. They limit injection rates whenever an instantaneous dose equivalent to about 1 Rad/day is exceeded.

The SVT employs a different strategy and circuitry to assess whether the measured radiation

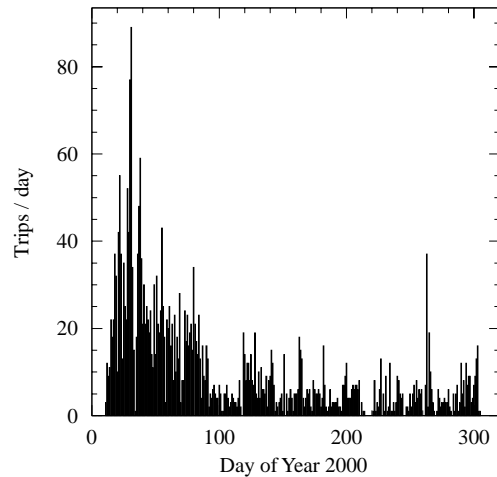


Figure 8. Daily rates of beam aborts initiated by the SVT radiation protection diodes, summed over regular data-taking and PEP-II injection.

levels merit a beam abort or a reduction in single-beam injection rate. Every beam dump initiated by *BABAR* is followed by a 10–15 minute period of injection with significant radiation exposure. Thus, to minimize the ratio of the integrated radiation dose to the integrated luminosity, it has been beneficial to tolerate transient high-dose events as long as the integrated dose remains less than the typical dose accumulated during injection. To differentiate between very high instantaneous radiation and sustained high dose rates, trip thresholds are enforced on two different time scales: an instantaneous dose of 1 Rad accumulated over 1 ms, and an average of 50 mRad/s measured over a 5-minute period. During injection, higher thresholds are imposed, since an aborted injection will delay the return to taking data.

Figure 8 shows the daily rate of beam aborts initiated by the SVT protection diodes during the year 2000. Initially, as many as 80 beam aborts were triggered per day, while the average for stable operation was significantly below ten at the end of the run. The measures described above, combined with a significant reduction in large background fluctuations, have been very effective in protecting the detector against radiation damage, as well increasing the combined live time of

the machine and detector to greater than 75%.

3.6. Impact of Beam-Generated Background on *BABAR*

Beam-generated backgrounds affect the detector in multiple ways. They cause radiation damage to the detector components and the electronics and thus may limit the lifetime of the experiment. They may also cause electrical breakdown and damage or generate large numbers of extraneous signals leading to problems with bandwidth limitations of the data acquisition system and with event reconstruction. Backgrounds can degrade resolution and decrease efficiency.

The impact of the beam-generated background on the lifetime and on the operation of the different detector systems varies significantly. Table 3 lists the limits on the instantaneous and integrated background levels in terms of the total dose and instantaneous observables. These limits are estimates derived from beam tests and experience of earlier experiments. For each detector system, an annual radiation allowance has been established taking into account the total estimated lifetime of the components and the expected annual operating conditions. The typical values accumulated for the first year of operation are also presented in the table.

Systematic studies of background rates were performed with stable stored beams. Measurements of the current-dependence of the backgrounds were carried out for single beams, two beams not colliding, and colliding beams with the goal to identify the principal background sources, to develop schemes of reducing these sources, and to extrapolate to operation at higher luminosity [16]. These experimental studies were complemented by Monte Carlo simulations of beam-gas scattering and of the propagation of showers in the detector. The studies show that the relative importance of the single-beam and luminosity background contributions varies, as illustrated in Figure 9. Data for the IFR are not shown because this system is largely insensitive to beam-generated backgrounds, except for the outer layer of the forward endcap, due to insufficient shielding of the external beam line components.

The experience of the first year of operation

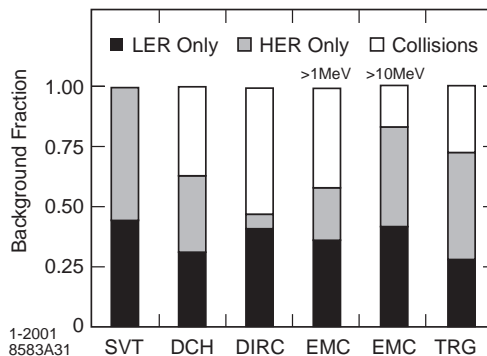


Figure 9. Fractional steady-state background contributions in *BABAR* detector systems, measured for single beams and colliding beams under stable conditions ($I^+ = 1.25$ A, $I^- = 0.75$ A, $L = 2.3 \times 10^{33}$ cm⁻² s⁻¹) in July 2000. The contributions are derived from the measured doses in the horizontal plane for the SVT, the total currents in the DCH, the rates in the DIRC photomultipliers, the occupancy and number of photons above 10 MeV in the EMC, and the L1 trigger rates.

and the concern for future operation for each of the detectors are summarized as follows.

SVT: The most significant concern for the SVT with regard to machine background is the integrated radiation dose. The instantaneous and integrated dose rates in the radiation protection diodes are representative, to within about a factor of two, of the radiation doses absorbed by the SVT modules. The exposure in the horizontal planes is an order of magnitude larger than elsewhere, averaging 15–25 mRad/s during stable beam operation. The highest integrated dose is 450 kRad, roughly 1 kRad/day. This dose is about 30% below the allowance, giving some confidence that the SVT can sustain operation for several more years (see Figure 7).

DCH: For the DCH, the currents on the wires are the main concern, both because of the limited capacity of the HV power supplies and the effect of wire aging. The currents drawn are approximately uniformly distributed among the 44 HV supplies, one for each quadrant of superlayers 2–10, and two per quadrant for superlayer 1.

Table 3

BABAR background tolerance. Operational limits are expressed either as lifetime limits (radiation-damage and aging-related quantities), or in terms of instantaneous observables (DCH current, DIRC and L1-trigger rates).

Detector system	Limiting factor and impact	Operational limit	First-year typical
SVT sensors and electronics	Integrated dose: radiation damage	2 MRad	0.33 MRad (hor.-plane modules) 0.06 MRad (other modules)
SVT sensors	Instantaneous dose: diode shorts	1 Rad/ms	N/A
DCH: electronics	Integrated dose: radiation damage	20 kRad	≤ 100 Rad
DCH: wire current	Accumulated charge: wire aging	100 mC/cm	8 mC/cm
DCH: total current	HV system limitations	1000 μ A	250 μ A (steady-state)
DIRC PMTs	Counting rate: TDC deadtime	200 kHz	110 kHz (steady-state, well-shielded sector)
EMC crystals	Integrated dose: radiation damage	10 kRad	0.25 kRad (worst case)
L1 trigger	Counting rate: DAQ dead time	2 kHz	0.7 kHz (steady-state)

Consequently, the total current limit is close to the sum of the limits of the individual supplies. During stable operation the total chamber current is 200–300 μ A. However, radiation spikes can lead to currents that occasionally exceed the limit of 1000 μ A, causing HV supplies to trip. Other background effects are measured to be well below the estimated lifetime limits and thus are not a serious issue at this time. The average wire occupancy has not exceeded 1–2% during stable operation, but the extrapolation to future operation at higher luminosity and currents remains a major concern.

DIRC: The DIRC radiators, made of synthetic fused silica, were tested up to doses of 100 kRad without showing any measurable effects and thus radiation damage is not a concern. The present operational limit of the DIRC is set by

the TDC electronics which induce significant dead time at rates above 250 kHz, well above the stable beam rate of 110 kHz in well shielded areas. Roughly half of the present rate is luminosity-related and can be attributed to radiative Bhabha scattering. The counting rate is due to debris from electromagnetic showers entering the water-filled *stand-off box*. Efforts are underway to improve the shielding of the beam pipe nearby.

EMC: The lifetime of the EMC is set by the reduction in light collection in the CsI crystals due to radiation damage. The cumulative dose absorbed by the EMC is measured by a large set of RadFETs placed in front of the barrel and end-cap crystals. RadFETs [18] are realtime integrating dosimeters based on solid-state Metal Oxide Semiconductor (MOS) technology. The absorbed dose increases approximately linearly with the in-

tegrated luminosity. The highest dose to date was observed in the innermost ring of the endcap, close to 250 Rad, while the barrel crystals accumulated about 80 Rad. The observed reduction in light collection of 10–15% in the worst place, and 4–7% in the barrel, is consistent with expectation (see Section 9).

The energy resolution is dependent on the single crystal readout threshold, currently set at 1 MeV. During stable beam conditions the average crystal occupancy for random triggers is 16%, with 10% originating from electronics noise in the absence of any energy deposition. The spectrum of photons observed in the EMC from the LER and HER is presented in Figure 10. The HER produces a somewhat harder spectrum. The average occupancy for a threshold of 1 MeV and the average number of crystals with a deposited energy of more than 10 MeV are shown in Figure 11 as a function of beam currents for both single and colliding beams. The occupancy increases significantly at smaller polar angles, in the forward endcap and the backward barrel sections, and in the horizontal plane. The rate increase is approximately linear with the single beam currents. Background rates recorded with separated beams are consistent with those produced by single beams. For colliding beams, there is an additional flux of photons originating from small angle radiative Bhabha scattering. This effect is larger for low energy photons and thus it is expected that at higher luminosities the low energy background will raise the occupancy and thereby limit the EMC energy resolution.

L1 Trigger: During stable beam operation, the typical L1 trigger rate is below 1 kHz, more than a factor of two below the data acquisition bandwidth limit of about 2.0–2.5 kHz. Experience shows that background bursts and other rate spikes can raise the data volume by as much as a factor of two and thus it is necessary to aim for steady state rates significantly below the stated limit. For the L1 trigger, the dominant sources of DCH triggers are particles generated by interactions in vacuum flanges and the B1 magnets (see Figure 86 in Section 11). This effect is most pronounced in the horizontal plane. At present, the HER background is twice as high as that of

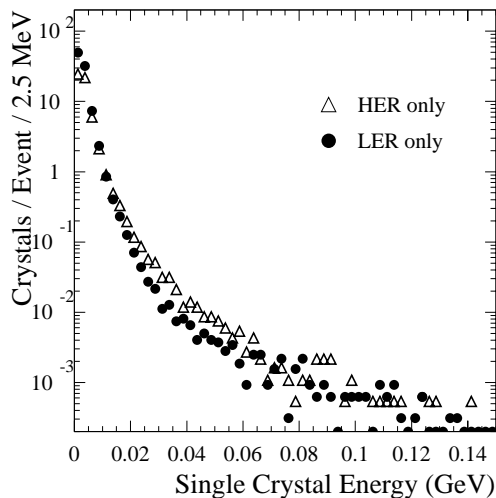


Figure 10. The energy spectrum of photons recorded in the EMC by random triggers with single beams at typical operating currents, LER at 1.1A and HER at 0.7A. The electronic noise has been subtracted.

the LER, and the colliding beams contribute less than half of the combined LER and HER single beam triggers.

3.7. Summary and Outlook

Towards the end of the first year of data-taking, PEP-II routinely delivered beams close to design luminosity. Due to the very close cooperation with the PEP-II operations team, the machine-induced backgrounds have not been a major problem once stable conditions were established. The background monitoring and protection system has become a reliable and useful tool to safeguard the detector operation.

Currently planned upgrades are expected to raise the luminosity to $1.5 \times 10^{34} \text{ cm}^{-2} \text{ s}^{-1}$ within a few years. The single beam backgrounds will increase with beam currents and the luminosity background is projected to exceed, or at best remain comparable to, the beam-gas contribution. Measures are being prepared to reduce the sources and the impact of machine-related background on *BABAR*, among them upgrades to the DCH power supply system and to the DIRC TDC electronics, the addition of localized shield-

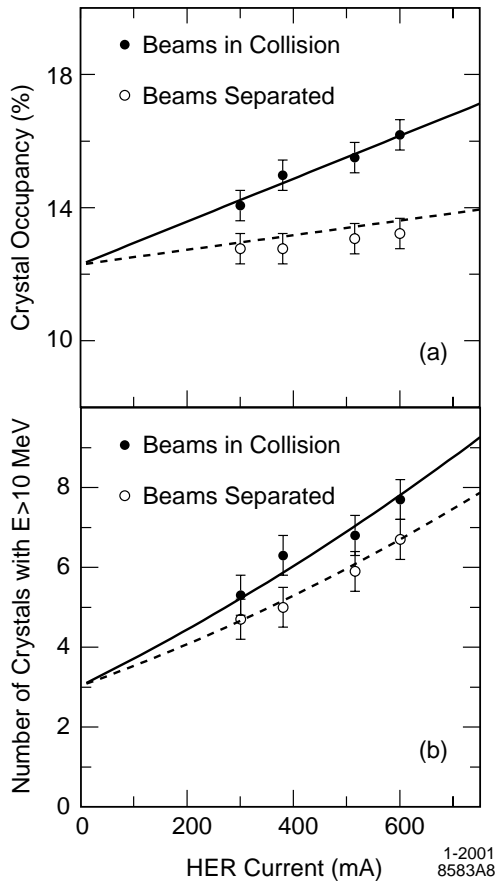


Figure 11. Average rates in the EMC for random triggers as a function of the HER current for a fixed LER current of 1.1A, both for separated and colliding beams; a) the single crystal occupancy for thresholds of 1 MeV and b) the number of crystals with a deposited energy greater than 10 MeV. The solid curves represent a fit to the colliding beam data, the dashed curves indicate the sum of rates recorded for single beams.

ing against shower debris (especially for the DIRC *stand-off box*), new vacuum chambers, adjustable collimators, and additional pumping capacity in critical regions upstream of the interaction point.

With the expected increase in LER current and in luminosity, both the single-beam and the luminosity-generated L1 trigger rates will increase and are projected to exceed 2 kHz (see Figure 12). Therefore, the DCH trigger is being up-

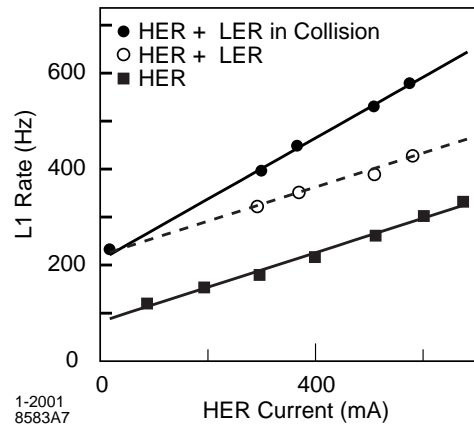


Figure 12. The L1 trigger rate as a function of the HER current for single beam only, for both beams, separated and colliding (with a LER current of 1.1A).

graded to improve the rejection of background tracks originating from outside the luminous region. In addition, the data acquisition and data processing capacity will need to be expanded to meet the demands of higher luminosity.

Overall, the occupancy in all systems, except the IFR, will probably reach levels that are likely to impact the resolution and reconstruction efficiency. For instance, the occupancy in the EMC is expected to more than double. Thus, beyond the relatively straight forward measures currently planned for *BABAR* system upgrades, detailed studies of the impact of higher occupancy will be necessary for all systems.